Enhanced Open-Circuit Voltage in High Performance Polymer/Fullerene Bulk-Heterojunction Solar Cells by Cathode Modification with a C60 Surfactant

ARTICLE *in* ADVANCED ENERGY MATERIALS · JANUARY 2012

Impact Factor: 16.15 · DOI: 10.1002/aenm.201100522

4 AUTHORS, INCLUDING:

Hin-Lap Yip
South China University of Technology
120 PUBLICATIONS **6,580** CITATIONS
SEE PROFILE

Alex K-Y Jen
University of Washington Seattle
391 PUBLICATIONS **15,458** CITATIONS
SEE PROFILE

COMMUNICATION

Enhanced Open-Circuit Voltage in High Performance Polymer/Fullerene Bulk-Heterojunction Solar Cells by Cathode Modification with a C_{60} Surfactant

*Kevin M. O'Malley, Chang-Zhi Li, Hin-Lap Yip, and Alex K.-Y. Jen**

Polymer solar cells (PSCs) represent a unique alternative renewable energy source combining the potential benefits of comparatively low-cost fabrication, solution processing, and wide application through the versatility of device design.[1,2] The advantages demonstrated by PSCs over their inorganic counterparts have generated extensive research efforts over the past decade, which have resulted in an impressive body of literature detailing vast improvements in device performance made through molecular design[3–7] and process and device engineering.[3,8–10] Power conversion efficiencies (PCEs) over 7% have recently been reported for bulk-heterojunction (BHJ) type PSCs due to significant strides in polymer design and morphological control of the photoactive blend.[7] Despite these promising advances, there remain a variety of technical issues to be addressed in order for PSCs to mature.

The most obvious of these issues is the significantly lower photovoltaic performance as compared to traditional silicon-based and dye-sensitized solar cells. One of the most critical factors determining device performance is the nature of the active layer/electrode interface, which has particularly important implications for the open-circuit voltage (V_{OC}).[11] In contrast to bilayer solar cells, the photoactive layer of BHJ PSCs typically consists of intimately mixed domains of *p*-type semiconducting polymer donor and *n*-type fullerene acceptor such that a bicontinuous pathway for charge transport through the layer to the electrodes is achieved. In the ideal case, the polymer and fullerene domains are sufficiently phase-segregated along the vertical charge-carrier transport axis which results in having only electron-(hole-)transporting material at the cathode (anode).[12] Due to the inherently complicated drying dynamics of the photoactive blend layer upon spin-coating, this is often not the case,[13,14] and the device performance suffers accordingly via charge recombination at the electrode interfaces.

In addition, proper energy level alignment at these interfaces is critical to reduce contact resistance and ensure a maximum V_{OC} and optimized device performance. To this end, several approaches have been employed to modify the organic/electrode interface. One method involves deliberate inclusion and/or tuning of a dipole layer to improve alignment between the Fermi level (E_F) of the contact and the appropriate frontier molecular orbital level of the organic, while another entails insertion of a thin layer of polymer surfactant to reduce contact resistance.[15–18] In conventional BHJ-based PSCs, the conducting polymer poly(ethylenedioxythiophene):poly(styrenesulfonate) (PEDOT:PSS) is used to modify the surface of the hole-collecting anode. With a work function (WF) closely matching the hole-transport level of a wide range of donor polymers, of the order of 5 eV below vacuum, PEDOT:PSS is capable of forming excellent electrical contact with the organic active layer of the device at the anode. Therefore, much attention has been paid to engineering the energy level alignment at the organic/cathode interface in efforts to improve device performance.

Recently, it has been reported that the performance of conventional PSC devices was increased due to spontaneous phase segregation of a polymer–fullerene blend by addition of fluorocarbon modified [6,6]-phenyl-C_{60}-butyric acid methyl ester (F-PCBM).[15] Upon spin-coating the blend, the fluorocarbon chain of the F-PCBM aligned at the organic/air interface creating a fullerene rich buffer layer for subsequent deposition of the cathode metal. Similar buffer layer formation via self-assembly has been achieved by adding fullerene-end-capped poly(ethylene glycol) (PEG-C_{60}) to the BHJ layer of PCBM and poly(3-hexylthiophene) (P3HT).[19,20]

We have recently synthesized a new bis-adduct fullerene surfactant (C_{60}-bis) that functions as an efficient electron selective material when inserted between various BHJ layers and an Al cathode, which led to improved performance in organic photovoltaic devices.[21] To better understand the origin of efficiency enhancement when C_{60}-bis is incorporated into PSCs, we have studied the electronic properties at the BHJ/C_{60}-bis/metal interface. We have performed the study based on a higher performance, low-bandgap polymer poly(indacenodithiophene-*co*-phananthrene-quinoxaline) (PIDT-PhanQ)[22] (**Figure 1**a) and [6,6]-phenyl-C_{71}-butyric acid methyl ester ($PC_{71}BM$) BHJ system and have investigated the effect of different cathode metals (Al, Ag, and Cu) on the PCE and stability of the PSCs. Because C_{60}-bis (Figure 1b) is processed from a methanol solution, there is no degradation of the underlying PIDT-PhanQ:$PC_{71}BM$ active layer. This device architecture (Figure 1c) effectively achieves the aforementioned desired phase-segregation (i.e., no polymer is in contact with the electron collecting electrode). Figure 1d shows the energy level diagram for the completed device. The highest occupied molecular orbital (HOMO) level of the surfactant is sufficiently deeper than that of the polymer, effectively

K. M. O'Malley, Prof. A. K.-Y. Jen
Department of Chemistry
University of Washington
Box 351700, Seattle, WA 98195, USA
E-mail: ajen@uw.edu
Dr. C.-Z. Li, Dr. H.-L. Yip, Prof. A. K.-Y. Jen
Department of Materials Science and Engineering
University of Washington
Box 352120, Seattle, WA 98195, USA

DOI: 10.1002/aenm.201100522

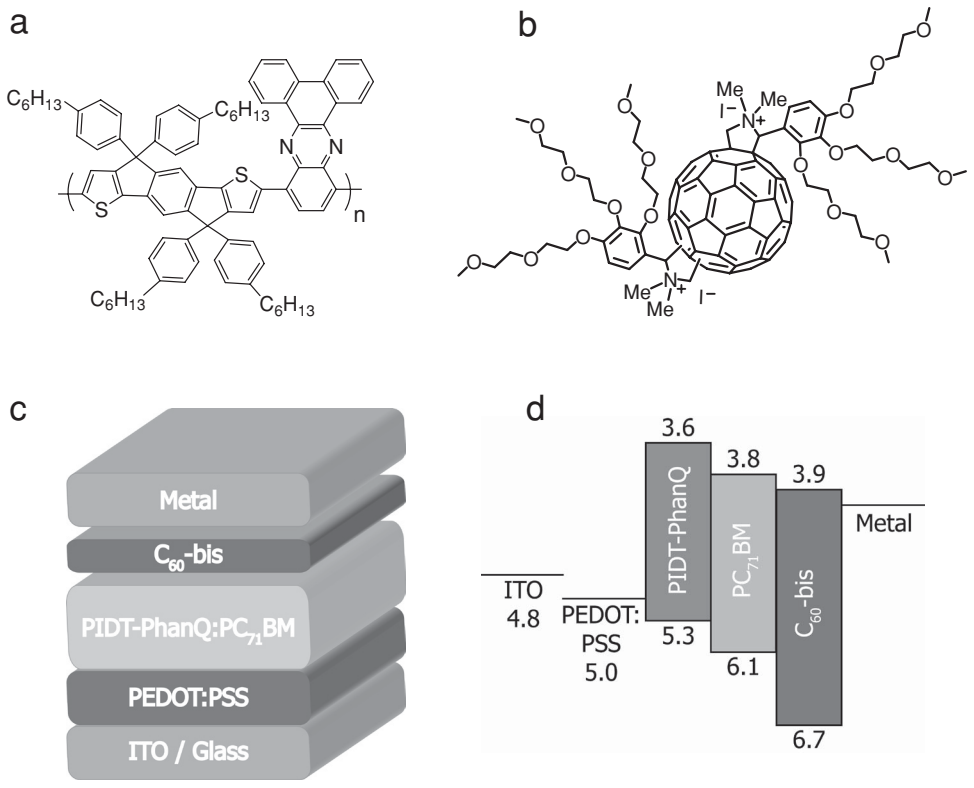

Figure 1. a) Chemical structures of PIDT-PhanQ and b) C_{60}- bis; and the conventional device architecture (c) with corresponding energy level diagram (d).

blocking holes generated in the photoactive layer from reaching the cathode and potentially recombining with electrons before they can be collected. This is evidenced by an increase in short-circuit current density (J_{SC}).

In addition, it has been proposed that the difference between the HOMO of the donor polymer and the lowest unoccupied molecular orbital (LUMO) of the acceptor fullerene in the photoactive layer, or more accurately the difference between the hole and electron quasi-Fermi levels, represents an estimate of the upper bound for the device V_{OC}.[23] In reality, the V_{OC} is usually smaller than this and is at best, assuming Ohmic contact at both electrodes, dictated by the difference between electrode WFs. Consequently, it is desirable to use a low-WF metal such as Al as the cathode material; however, such metals are easily oxidized in air eventually leading to degradation of device performance.[24] To circumvent this issue, we have fabricated devices with higher WF metals less prone to oxidation, which are shown to perform better than Al devices over time. Remarkably, the V_{OC} appears to be independent of the choice of cathode metal when C_{60}-bis is used as a buffer layer.

Figure 2a shows the *J–V* characteristics for devices fabricated with different cathode metals both with and without a C_{60}-bis buffer layer. The V_{OC} for devices with an Al cathode is consistently lower than that of Cu and Ag devices, which can be attributed to the rapid oxidation of Al in air. The nonideal nature of this interface also manifests in a modest fill factor (FF) of 0.51 and an overall PCE of 3.22%. In contrast, when a layer of C_{60}-bis is used, the PCE increases to 5.87% as a result of an increase in J_{SC}, FF, and most notably V_{OC}. In addition, the shunt resistance is shown to increase for all metals in the case of C_{60}-bis, which provides evidence of lower leakage current under illumination. Performance data for all devices are summarized in **Table 1**.

To investigate the improvement in J_{SC}, external quantum efficiency (EQE) spectra (Figure 2b) were obtained for Al, Ag, and Cu devices. The spectra exhibit an almost constant increase across the entire wavelength range for each case when the surfactant layer was inserted. This indicates the improvement in J_{SC} is due entirely to the inclusion of the surfactant and a concurrent decrease in recombination at the organic/electrode interface, rather than a change in bulk morphology.

To further demonstrate the utility of C_{60}-bis as an interfacial layer, the PCE of devices with different cathode metals were tracked over a period of time under exposure to ambient conditions. **Figure 3** shows the normalized PCE for unencapsulated devices with and without C_{60}-bis over 100 h in air. As expected, the performance of Al devices drops off rapidly, even with the inclusion of the fullerene surfactant, which is likely due to the uptake of oxygen and water molecules and their subsequent diffusion to the metal/organic interface. The Ag and Cu devices remain very stable, however, with the Cu/C_{60}-bis retaining nearly 90% of its original PCE after the entire period of ambient exposure.

By far, the most obvious benefit of C_{60}-bis is a strongly enhanced V_{OC}. To further investigate the dramatic increase in V_{OC} when C_{60}-bis is used, capacitance–voltage characteristics (*C–V*) were obtained and devices were analyzed via

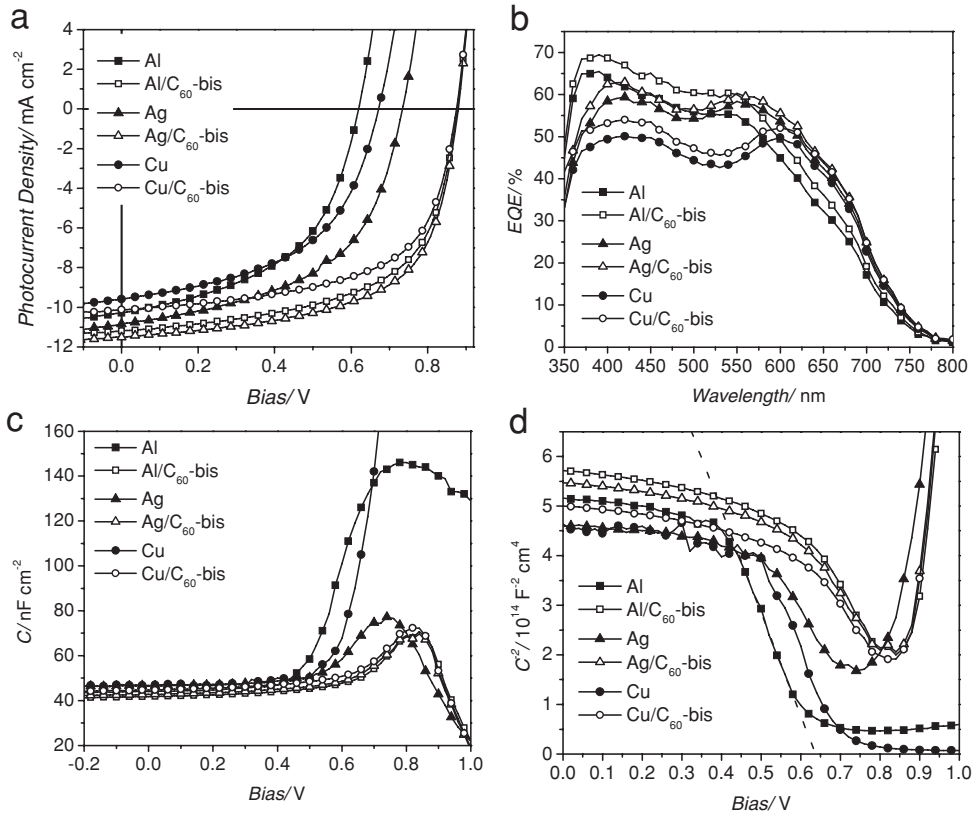

Figure 2. Performance data for PIDT-PhanQ:$PC_{71}BM$ devices fabricated with different choice of cathode metal with and without a C_{60}-bis interlayer. The current density–voltage curves a) and external quantum efficiency spectra b) show increases in V_{OC} and J_{SC}, respectively. c) Capacitance–voltage and d) Mott–Schottky analysis explain increased V_{OC} in terms of the V_{BI} of the Schottky contact.

Mott–Schottky (MS) analysis. It has previously been shown that, due to the intrinsic *p*-doped nature of semiconducting polymers, a Schottky contact is formed upon deposition of the cathode onto the photoactive layer.[25] The depletion zone formed at this interface is modulated by the applied voltage under reverse and low (<1.5 V) forward bias. Boix et al.[26] showed that band-bending results in the vicinity of the cathode, allowing extraction of the built-in potential (V_{BI}) and impurity concentration (N) of the region by application of $C^{-2} = (2/q\varepsilon N)(V_{BI} - V)$ to the appropriate bias voltage range.

Figure 2c shows the capacitance behavior of all devices as a function of bias voltage. The low-capacitance region up to about 0.5 V has been attributed to the capacitance of the depletion layer, whereas a further increase in forward bias voltage yields a peak in the capacitance related to the storage of minority carriers in the bulk.[27] Figure 2d shows the MS plot for all fabricated

Table 1. Summary of performance data for PIDT-PhanQ:$PC_{71}BM$ devices with different cathode metals, with and without C_{60}-bis.

Device	V_{OC} [V]	J_{SC} [mA cm^{-2}]	FF	PCE [%]	R_{SH} [Ω cm^{-2}]
Al	0.62	10.28	0.51	3.22	309.33
Al/C_{60}-bis	0.88	11.19	0.60	5.87	773.33
Ag	0.73	10.83	0.53	4.22	351.63
Ag/C_{60}-bis	0.88	11.50	0.61	6.22	662.86
Cu	0.67	9.58	0.51	3.32	386.67
Cu/C_{60}-bis	0.87	10.13	0.61	5.37	795.43

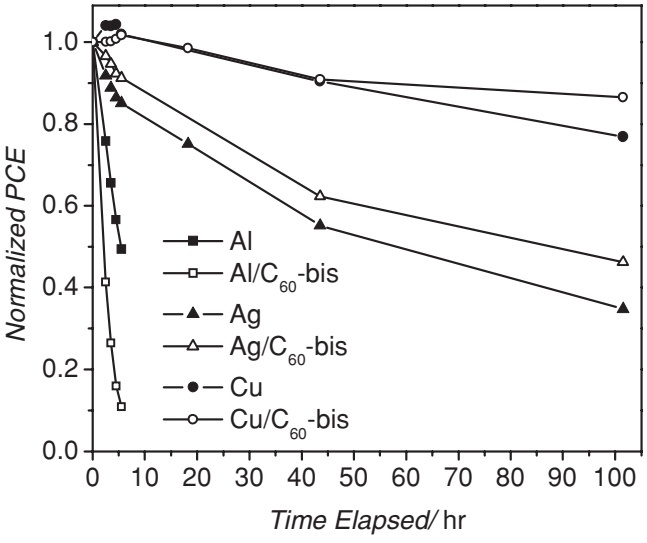

Figure 3. Normalized PCE for Al, Ag, and Cu devices with and without C_{60}-bis under ambient conditions.

Table 2. Summary of the built-in potential V_{BI}, dopant concentration N, and depletion width w of the organic/cathode Schottky contact from Mott – Schottky analysis. The work functions and relative shifts in V_{OC} and V_{BI} for all devices are also included.

Device	V_{OC} [V]	V_{BI} [V]	(ΔV_{OC}, ΔV_{BI}) [V]	N [10^{16} cm^{-3}]	w [nm]	$\Phi_{cathode}$ [eV]
Al	0.619	0.636	–	2.25	97	4.25
Al/C_{60}-bis	0.877	0.940	(0.26, 0.30)	3.32	97	3.66
Ag	0.734	0.808	–	3.39	89	4.57
Ag/C_{60}-bis	0.879	0.959	(0.15, 0.15)	3.77	92	3.97
Cu	0.672	0.712	–	2.51	97	4.70
Cu/C_{60}-bis	0.875	0.957	(0.20, 0.25)	4.02	89	3.96

devices. At moderate to high reverse bias, C^{-2} tends to reach a steady value related to the geometric capacitance of the organic material which has become fully depleted of majority carriers and can be viewed as a classical dielectric. As previously mentioned, the linear region under low forward bias is related to the formation of a Schottky contact and can be fitted to a plot of C^{-2} versus bias voltage. Extrapolation of the linear fit line to the intercept on the bias axis directly yields V_{BI} for the device. Once a value for V_{BI} has been obtained, an impurity concentration N and depletion width $w = (2\varepsilon V_{BI}/qN)^{1/2}$ corresponding to zero applied bias can be extracted.[26,28] A dielectric permittivity of 3 has been assumed for calculations involving these equations.[28] MS analysis data, along with the relative shifts in V_{OC} and V_{BI}, are summarized in **Table 2**.

Interestingly, the depletion width extracted from the capacitance–voltage data extends over almost the entire thickness of the active layer. When taken with the values of N obtained from the same data, this indicates a consistent doping profile across the entire layer that changes negligibly by inclusion of C_{60}-bis. Since the change in the Fermi level of the active layer (E_F^p) can be approximated by $\Delta E_F^p = k_b T \ln(N_b/N_a)$,[28] where N_b and N_a are the dopant concentrations of the device with and without C_{60}-bis, respectively, it is reasonable to conclude that E_F^p does not change more than ≈10 meV. When a semiconductor is placed in intimate contact with a metal, their respective E_F come into equilibrium by electrons being transferred "downhill" in energy.[29,30] If we reference V_{BI} to E_F^p by $V_{BI} = (E_F^p - \Phi_{cathode})$, where $\Phi_{cathode}$ is the cathode WF, then the difference in V_{BI} with and without C_{60}-bis can be attributed to a modification of $\Phi_{cathode}$ by the surfactant.[31] Furthermore, because the relative shifts in V_{BI} closely follow those of V_{OC} for all three metals, we can conclude that the observed increase in V_{OC} upon inclusion of C_{60}-bis is due to a dipole-induced shift in $\Phi_{cathode}$ at the interface.

To further investigate the energetics at the interface, WFs were obtained for Al, Ag, and Cu with and without C_{60}-bis spin-coated on top and are summarized in Table 2. WFs of in situ, sputter-cleaned Al, Ag, and Cu films were measured to be 4.25, 4.57, and 4.70 eV, respectively (Figure S2, Supporting Information). Interestingly, the WFs of Ag and Cu with C_{60}-bis yield nearly the same value. Since sampling of the substrate at normal emission is highly surface sensitive, it is reasonable to assume these WF values correspond to the C_{60}-bis. As the material is an *n*-type semiconductor, one would expect E_F to be closer to the LUMO level than midgap, which matches well with our findings. It should be noted that the WFs of the organic overlayer may not be measured in the flat-band condition, but are rather subject to any band bending occurring at the metal/organic interface as a result of E_F equilibration. In addition, it is likely that an unavoidable thin oxide layer formed on the Al sample when it was removed from the glovebox for C_{60}-bis deposition, as evidenced by a comparison of oxygen 1s peak intensity in X-ray photoelectron survey spectra for bare Al before and after sputter-cleaning with Ar^+ ions. These considerations might explain the lower WF of the modified Al cathode compared to Ag and Cu.

It should be stressed that these conditions do not prevail for regular device fabrication because the cathode is deposited under high vacuum after spin-coating the C_{60}-bis layer outside the glovebox. Regardless, at a distance sufficiently far into the bulk of the photoactive layer only the effective WF of the C_{60}-bis modified cathode can be "seen" by the rest of the device. This ensures a constant difference between E_F^p and $\Phi_{cathode}$, and explains why V_{BI}, and consequently V_{OC}, is nearly the same for all three metals when C_{60}-bis is employed.

In conclusion, a C_{60} bis-adduct surfactant was used to modify the energy level alignment at the organic/cathode interface in conventional structure, BHJ PSC devices. A well-defined interface between the photoactive layer and the surfactant was ensured by virtue of process solvent orthogonality. The large increase in device V_{OC} is independent of the choice of cathode metal due to pinning of the metal E_F to that of C_{60}-bis upon equilibration. MS analysis of the interface formed between the photoactive layer and the cathode yields a built-in potential defined by the difference between the Fermi level of the BHJ E_F^p and the effective cathode WF $\Phi_{cathode}$. The observed changes in V_{BI} are reflected in the magnitude of the change in V_{OC}. Further, EQE data reveal the overall device performance enhancement to be due entirely to the inclusion of the surfactant, rather than a beneficial change in photoactive layer morphology.

Experimental Section

Fabrication of Photovoltaic Devices: Indium tin oxide (ITO)-coated glass substrates (15 Ω sq^{-1}) were cleaned sequentially by sonication in detergent and deionized water, acetone, and isopropanol. After drying under a N_2 stream, substrates were air–plasma treated for 30 s. A ≈35 nm layer of PEDOT:PSS (Baytron P VP Al 4083, filtered through a 0.45 µm nylon filter) was spin-coated onto the clean substrates at 5 k rpm and annealed at 140 °C for 10 min. The substrates were transferred to a N_2-filled glovebox where a homogeneously blended solution of PIDTPhanQ:PC_{71}BM (40 mg mL^{-1} in *o*-dichlorobenzene stirred overnight in glovebox, 1:3 polymer:fullerene by weight) was spin-coated at 2 k rpm, producing an active layer ≈100 nm thick, and annealed at 110 °C for 10 min. Substrates requiring a layer of fullerene surfactant were briefly transferred out of the glovebox (total ambient exposure <10 min) and a ≈2–5 nm thick film of C_{60}-bis surfactant (1 mg mL^{-1} in methanol) was spin-coated at 5 k rpm. The substrates were then transferred back into the glovebox and annealed at 110 °C for 5 min to drive off any remaining solvent prior to metal deposition. Metal electrodes were deposited at a base pressure <1 × 10^{-6} Torr through a shadow mask, defining an active device area of 4.64 mm^2. Ag and Cu were deposited at a rate of 1 Å s^{-1} and Al was deposited at a rate of 4 Å s^{-1}.

Preparation of XPS Samples: ITO-coated glass substrates were prepared as above sans air–plasma treatment. Al, Ag, and Cu were deposited over the entire substrate surface at a rate of 1 Å s^{-1}. Substrates requiring a thin layer of fullerene surfactant were transferred out of the glovebox and a solution of C_{60}-bis surfactant was spin-coated from methanol using the same conditions as above. After transfer back into the glovebox, all substrates were heated at 70 °C for 5 min to evaporate any remaining methanol prior to being sealed with parafilm in 20 mL glass vials under N_2 for transport to the XPS.

Measurement and Characterization: *J–V* characteristics of the unencapsulated devices were measured in ambient conditions using a Keithley 2400 source meter under AM 1.5 G (100 mW cm^{-2}) irradiation simulated by an Oriel xenon lamp (450 W). AM 1.5 G illumination was confirmed by means of calibration to a standard silicon photodiode (Hammamatsu) which can be traced to the National Renewable Energy Laboratory. EQE spectra were obtained by measuring the photocurrent response of the device using chopped, monochromated light from the same xenon lamp in conjunction with a Stanford Research Systems SR830 lock-in amplifier under ambient conditions. MS analysis was performed in a N_2-filled glovebox in the dark using a Signatone probe station interfaced with an Agilent HP4284A precision LCR meter. The 1 kHz AC signal applied during measurement was kept at an amplitude of 25 mV to maintain response linearity. Capacitance-voltage characteristics measured thusly were obtained using devices prepared as above with an active area of 10.08 mm^2. WF determination via XPS is described in detail in the Supporting Information. Briefly, the secondary electron cutoff (SEC) spectrum of each sample was measured under ultra-high vacuum ($<5 \times 10^{-9}$ Torr) using a PHI 5000 VersaProbe (Ulvac-Phi, Inc.) employing a focused, monochromated Al K-α X-ray source and a hemispherical analyzer. Proper referencing of the SEC edge to that of Ar^+ ion sputter-cleaned, polycrystalline gold allowed for accurate determination of the sample WFs with a reproducibility of about 0.05 eV.

Supporting Information

Supporting Information is available from the Wiley Online Library or from the author.

Acknowledgements

The authors would like to acknowledge support from NSF (STC-DMR-0120967), DOE (DEFC3608GO18024/A000), AFOSR (FA9550-09-1-0426), ONR (N00014-11-1-0300), and the World Class University program through National Research Foundation of Korea (R31-21410035). AKYJ thanks the Boeing Foundation for support.

Received: September 3, 2011
Revised: October 25, 2011
Published online: December 5, 2011

[1] G. Dennler, M. C. Scharber, C. J. Brabec, *Adv. Mater.* **2009**, *21*, 1323.
[2] F. C. Krebs, *Sol. Energy Mater. Sol. Cells* **2009**, *93*, 394.
[3] S. H. Park, A. Roy, S. Beaupré, S. Cho, N. Coates, J. S. Moon, D. Moses, M. Leclerc, K. Lee, A. J. Heeger, *Nat. Photon.* **2009**, *3*, 297.
[4] H.-Y. Chen, J. Hou, S. Zhang, Y. Liang, G. Yang, Y. Yang, L. Yu, Y. Wu, G. Li, *Nat. Photon.* **2009**, *3*, 649.
[5] R. Qin, W. Li, C. Li, C. Du, C. Veit, H.-F. Schleiermacher, M. Andersson, Z. Bo, Z. Liu, O. Inganas, U. Wuerfel, F. Zhang, *J. Am. Chem. Soc.* **2009**, *131*, 14612.
[6] Y. He, H.-Y. Chen, J. Hou, Y. Li, *J. Am. Chem. Soc.* **2010**, *132*, 1377.
[7] Y. Liang, Z. Xu, J. Xia, S.-T. Tsai, Y. Wu, G. Li, C. Ray, L. Yu, *Adv. Mater.* **2010**, *22*, E135.
[8] J. Peet, J. Y. Kim, N. E. Coates, W. L. Ma, D. Moses, A. J. Heeger, G. C. Bazan, *Nat. Mater.* **2007**, *6*, 497.
[9] J. Y. Kim, K. Lee, N. E. Coates, D. Moses, T.-Q. Nguyen, M. Dante, A. J. Heeger, *Science* **2007**, *317*, 222.
[10] C. J. Brabec, S. E. Shaheen, C. Winder, N. S. Sariciftci, P. Denk, *Appl. Phys. Lett.* **2002**, *80*, 1288.
[11] K. Vandewal, K. Tvingstedt, A. Gadisa, O. Inganäs, J. V. Manca, *Nat. Mater.* **2009**, *8*, 904.
[12] A. Kumar, G. Li, Z. Hong, Y. Yang, *Nanotechnology* **2009**, *20*, 165202.
[13] D. S. Germack, C. K. Chan, B. H. Hamadani, L. J. Richter, D. A. Fischer, D. J. Gundlach, D. M. DeLongchamp, *Appl. Phys. Lett.* **2009**, *94*, 233303.
[14] Z. Xu, L.-M. Chen, G. Yang, C.-H. Huang, J. Hou, Y. Wu, G. Li, C.-S. Hsu, Y. Yang, *Adv. Funct. Mater.* **2009**, *19*, 1227.
[15] Q. Wei, T. Nishizawa, K. Tajima, K. Hashimoto, *Adv. Mater.* **2008**, *20*, 2211.
[16] H. Ma, H.-L. Yip, F. Huang, A. K.-Y. Jen, *Adv. Funct. Mater.* **2010**, *20*, 1371.
[17] S.-H. Oh, S.-I. Na, J. Jo, B. Lim, D. Vak, D.-Y. Kim, *Adv. Funct. Mater.* **2010**, *20*, 1977.
[18] Z. He, C. Zhang, X. Xu, L. Zhang, L. Huang, J. Chen, H. Wu, Y. Cao, *Adv. Mater.* **2011**, *23*, 3086.
[19] Q. Tai, J. Li, Z. Liu, Z. Sun, X. Zhao, F. Yan, *J. Mater. Chem.* **2011**, *21*, 6848.
[20] J. W. Jung, J. W. Jo, W. H. Jo, *Adv. Mater.* **2011**, *23*, 1782.
[21] C.-Z. Li, H.-L. Yip, S.-H. Oh, K. M. O'Malley, C.-C. Chueh, Y. Sun, Y. Zhang, N. Cho, A. K.-Y. Jen, unpublished.
[22] Y. Zhang, J. Zou, H.-L. Yip, K.-S. Chen, D. F. Zeigler, Y. Sun, A. K.-Y. Jen, *Chem. Mater.* **2011**, *23*, 2289.
[23] G. Garcia-Belmonte, J. Bisquert, *Appl. Phys. Lett.* **2010**, *96*, 113301.
[24] K. Lee, J. Y. Kim, S. H. Park, S. H. Kim, S. Cho, A. J. Heeger, *Adv. Mater.* **2007**, *19*, 2445.
[25] G. Garcia-Belmonte, A. Munar, E. M. Barea, J. Bisquert, I. Ugarte, R. Pacios, *Org. Electron.* **2008**, *9*, 847.
[26] P. P. Boix, M. M. Wienk, R. A.J. Janssen, G. Garcia-Belmonte, *J. Phys. Chem. C* **2011**, *115*, 15075.
[27] G. Garcia-Belmonte, A. Munar, E. M. Barea, J. Bisquert, I. Ugarte, R. Pacios, *Org. Electron.* **2008**, *9*, 847.
[28] P. P. Boix, J. Ajuria, I. Etxebarria, R. Pacios, G. Garcia-Belmonte, J. Bisquert, *J. Phys. Chem. Lett.* **2011**, *2*, 407.
[29] H. Ishii, K. Sugiyama, E. Ito, K. Seki, *Adv. Mater.* **1999**, *11*, 605.
[30] S. Braun, W. R. Salaneck, M. Fahlman, *Adv. Mater.* **2009**, *21*, 1450.
[31] J. Bisquert, G. Garcia-Belmonte, *J. Phys. Chem. Lett.* **2011**, *2*, 1950.